

Gouge Particle Evolution in a Rock Fracture Undergoing Shear: a Microscopic DEM Study

Zhihong Zhao

Received: 19 September 2012 / Accepted: 14 January 2013 / Published online: 9 February 2013
© Springer-Verlag Wien 2013

Abstract The evolution of gouge materials in rock fractures or faults undergoing shear can change fracture properties in terms of shear strength and dilation, fluid transmissivity and retardation for contaminants. In order to conceptually understand gouge mechanical behaviors including movement, microcracking, abrasion and redistribution, particle mechanics models were used to simulate single- and multi-gouge particles in a rough fracture segment undergoing shear. The results show that gouge particles behave in two different ways under low and high normal stresses, respectively. Under low normal stress, gouge particles mainly roll with the moving fracture walls, with little surface damage and small dilation during the shear process. Under high normal stress, gouge particles can be crushed into a few major pieces and a large number of minor comminuted particles, accompanied by more severe damage (abrasion and microcracking) in fracture walls and continuous fracture closure. The modeling results were also compared with published experiments and used to explain the observed macroscopic behaviors of rock fracture undergoing shear. The effects of microparameters used in the particle mechanics models on the simulation of gouge behaviors were also investigated through sensitivity analysis.

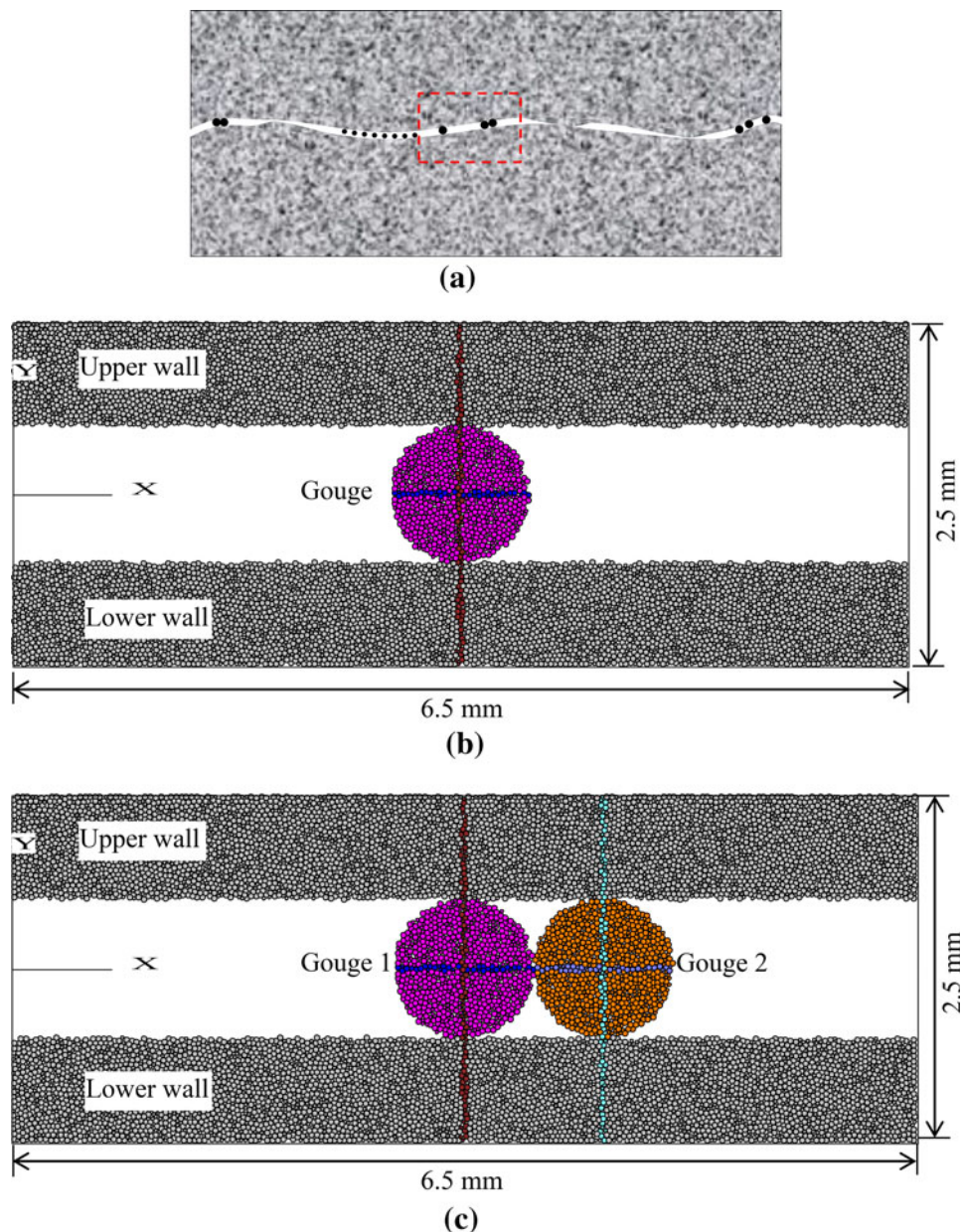
Keywords Gouge evolution · Rock fracture · Shear · Particle breakage · Surface damage · Particle mechanics model

1 Introduction

Gouge material (sheared-off or broken particles) is usually generated from rock fracture surfaces undergoing compression and shear, and subsequently these gouge particles can be further crushed into even smaller ones with increasing shear displacement or normal stresses. This can change the gouge particle size, position and distribution significantly (Sammis et al. 1987; Scholz 1987; Haggert et al. 1992; Pereira and de Freitas 1993). Therefore, the production and evolution of gouge material in rock fractures can play a key role in fracture mechanical and transport properties, e.g., friction coefficient, shear strength, fluid transmissivity and solute retardation coefficient (Jing and Stephansson 2007; Zhao et al. 2012). In addition, fracture surface damage (abrasion and microcrack development) can also be induced by gouge movements. However, the progress of research on the evolution behaviors of gouge material in rock fractures has been slow because of the technical difficulty in measuring the rate of gouge production, movement and distribution experimentally. The main objective of this study is to monitor and understand the gouge particle evolution (movement and breakage) in a rough rock fracture undergoing direct shear at a microscopic scale (red block in Fig. 1), using a particle mechanics model. Unlike previous studies, this study focused on a small segment of fracture filled in with one or two gouge particles instead of many gouge particles filling in a long fracture (or fault) (Pereira and de Freitas 1993; Mair and Abe 2008; Togo and Simamoto 2012). In this way, the processes of gouge particle evolution under different shear condition can be modeled and monitored clearly. The modeling results that exhibited similar behaviors observed in experiments provide implications for the macroscopical hydro-mechanical behaviors of rock fractures.

Z. Zhao (✉)
Department of Geological Sciences, Bolin Centre for Climate Research, Stockholm University, 10691 Stockholm, Sweden
e-mail: zhihong.zhao@geo.su.se

Fig. 1 Schematic view of rock fracture filled by gouge particles and particle mechanics models representing the gouge particles in a rock fracture segment (*red block* in **a**). Orthogonal markers were installed in the specimen to visualize the movement of the gouge and fracture wall, but their properties were the same as fracture walls and gouge particles regardless of the colors. **a** A sketch of rock fracture filled with gouge materials. **b** Single-gouge model. **c** Two-gouge model. **c** Two-gouge model (color figure online)



Particle mechanics models have recently been used to study the mechanical behaviors of single rock fractures during direct shear tests (Cundall 1999; Wang et al. 2003; Park and Song 2009; Asadi and Rasouli 2010; Duriez et al. 2010; Asadi et al. 2012), but the gouge production and evolution were not considered in the previous publications. For granular soils, particle mechanics models were also employed to simulate the breakage of crushable soil agglomerates (McDowell and Harireche 2002; Cheng et al. 2003; Lobo-Guerrero and Vallejo 2005; Wang and Yan 2011). Among them, Lobo-Guerrero and Vallejo (2005) proposed a scheme to replace the original particles that fulfill failure criterion with a set of smaller particles, but that replacement approach could not conserve mass balance. Those studies provide some useful understanding of

soil agglomerate breakage behaviors, but gouge particles in a rock fracture may exhibit different properties and evolution behaviors, which need further investigations. This is the motivation of the present study. As a first step to gain some insights, the mechanical and geometric properties of gouge particles were addressed in this study, but their effects on the transport properties of rock fractures are not considered.

2 Modeling Procedure

Two-dimensional (2D) particle flow code, PFC2D (Itasca Consulting Group Inc 2008), was used in this study. Basically, a PFC2D model represents the rock matrix by an

two-dimensional dense packing assembly of circular disks of non-uniform sizes, and the disks are bonded in the normal and shear directions at all contacts that possess finite (normal and shear) stiffness and (tensile and shear) strengths (Potyondy and Cundall 2004). Hereafter, to avoid confusion of terminology, the word ‘particle’ is used only for ‘gouge particles,’ but the word ‘ball’ refers to ‘particles’ in PFC2D models. The fracture segment (Fig. 1) consists of two sets of densely packed balls (gray color) of non-uniform sizes, and the two sets represent the upper and lower fracture walls, respectively. The gouge particles are represented by circular disks with a large number of bonded balls (Fig. 1). ‘Lump logic’ is not used for gouge particle crushing because the ‘lump particles’ are unbreakable (Park and Song 2009). The contacts representing interfaces between rocks and gouge particles are assigned zero bond strengths, but a nonzero friction coefficient. Other microparameters are the same for all the balls in the model. In this way, the roughness of both fracture and gouge surfaces can be naturally simulated by the arrangement of balls. Without repetition of basic assumptions and laws of particle flow that can be found in the literature (e.g., Itasca Consulting Group Inc 2008; Potyondy and Cundall 2004), this section mainly focuses on the model setup and modeling procedure of gouge evolution during the shear process. Note that PFC2D models used in this study refer to a thin slice of rock, so the width of the model can be understood as the same magnitude as the gouge particle radius. This assumption may or may not represent a strict theoretical plane strain model, but it is needed to facilitate the gouge particle volume calculation. Therefore, when referring to the gouge volume, one calculates the sum of the areas of the balls.

According to the basic specimen-genesis procedure in Potyondy and Cundall (2004) and Itasca Consulting Group Inc (2008), 15,000 particles were packed into a rectangular box with a length of 6.5 mm and a height of 2.5 mm to build up intact rocks, through four steps, i.e., compacting initial assembly, installing specified isotropic stress, removing ‘floating’ particles and installing contact bonds. The average ball radius was about 0.017 mm, with the maximum and minimum of 0.022 and 0.012 mm, respectively, and each ball had at least three contacts with other neighbor balls. All of the model parameters are listed in Table 1, the values of which were the same or similar to the literature pertaining to rock fractures modeled using PFC (Cundall 1999; Potyondy and Cundall 2004; Park and Song 2009, 2013; Asadi and Rasouli 2010; Asadi et al. 2012). The numerical biaxial and Brazilian tests (Itasca Consulting Group Inc. 2008) were carried out, demonstrating the microparameters can represent the properties of fresh rock fracture. The constant normal stresses on the upper walls were applied using the servo control algorithm

Table 1 Microparameters for the intact rocks of demonstration fracture samples

Parameter (unit)	Value	Comparison
Number of balls (–)	15,000	5,000, 10,000, 20,000
Ball density (kg/m ³)	2,600	
Ball-ball contact modulus (GPa)	5.0	0.5, 50
Ratio of ball shear to normal stiffness (–)	0.3	
Bond contact friction coefficient (–)	0.6	0.4, 0.5, 0.7, 0.8
Bond contact normal strength, mean (MPa)	20	10, 30
Bond contact normal strength, standard deviation (MPa)	5.0	
Bond contact shear strength, mean (MPa)	20	10, 30
Bond contact shear strength, standard deviation (MPa)	5.0	

(Itasca Consulting Group Inc 2008), and then the balls located in the middle part (fracture voids) of the rectangular box were removed to form gouge particles (Fig. 1). This means that the simulations began at the moment when gouge particles were produced (possibly by abrasion at asperity contacts). The radius of each gouge particle was about 0.5 mm and consisted of about 730 balls. During the direct shear test, the upper block of the specimen moved in the right direction at a final constant speed of 0.5 m/s under constant normal stress condition. This shearing speed was sufficiently low to ensure that the sample remained under a quasi-static equilibrium state during the shear process, and it was reached in a sequence of ten stages to avoid inertial forces within the specimen. The movement and breakage of gouge particles, microcrack development in gouge particles and fracture walls, fracture normal displacement of the upper wall (shear dilation was obtained if the upper wall moved above its original position) and shear stresses were monitored during the whole shear process and are presented in Sect. 3.

3 Results

Two cases were studied (Fig. 1). There was a single gouge particle or two interacting gouge particles within a rock fracture segment, respectively, under constant normal stresses of 0.225, 0.5, 0.75 and 1.0 MPa. After a large number of simulations, two basic types of gouge evolution can be categorized: (1) gouge particle rolling with gentle surface erosion under low normal stresses and (2) serious gouge breakage under high normal stress. These are presented in this section. The influences of microparameters on the simulations are described in the next section, so the

explanation in this section is based on the models with microparameters listed in the middle column of Table 1.

3.1 Single Gouge Particle Model

3.1.1 Gouge Behavior

Under constant normal stresses of 0.225 and 0.5 MPa, the gouge particles rolled with the moving wall, and the horizontal displacements of gouge centers were the same, about 0.56 mm after a shear displacement of 1.17 mm (Fig. 2a, b). Slight surface erosion (edge damage or abrasion) occurred at the bottom of the gouge particle, and discrete-distributed microcracks initiated inside the gouge particle and fracture walls under a normal stress of 0.5 MPa (Fig. 3a, b). The rotation angles were about 65° under normal stresses of 0.225 and 0.5 MPa. This can be used to calculate the shear displacement, i.e.,

$2\pi \times 0.5 \text{ mm} \times (65^\circ/180^\circ) = 1.13 \text{ mm}$. Compared with the shear displacement of 1.17 mm, the agreement indicates that the main type of gouge particle movement was rolling, and the particle movement pattern did not change for normal stress, increasing from 0.225 to 0.5 MPa, in spite of more surface damage. Figure 4 shows the intermediate rolling stages of a single gouge particle in the fracture void with the moving upper wall. When normal stress increased to 0.75 and 1.0 MPa, gouge particle breakage was observed after a shear displacement of 1.17 mm (Figs. 2c, d, 3c, d). However, the gouge particle still rolled at the beginning period of the shear process (before breakage), accompanied by microcracking inside the gouge particle and surface erosion (Fig. 5a). With increasing shear displacements, the microcracks fully propagated through the gouge particle and full breakage occurred (Fig. 5b). The original gouge particle was crushed into two and four major pieces under normal stresses of

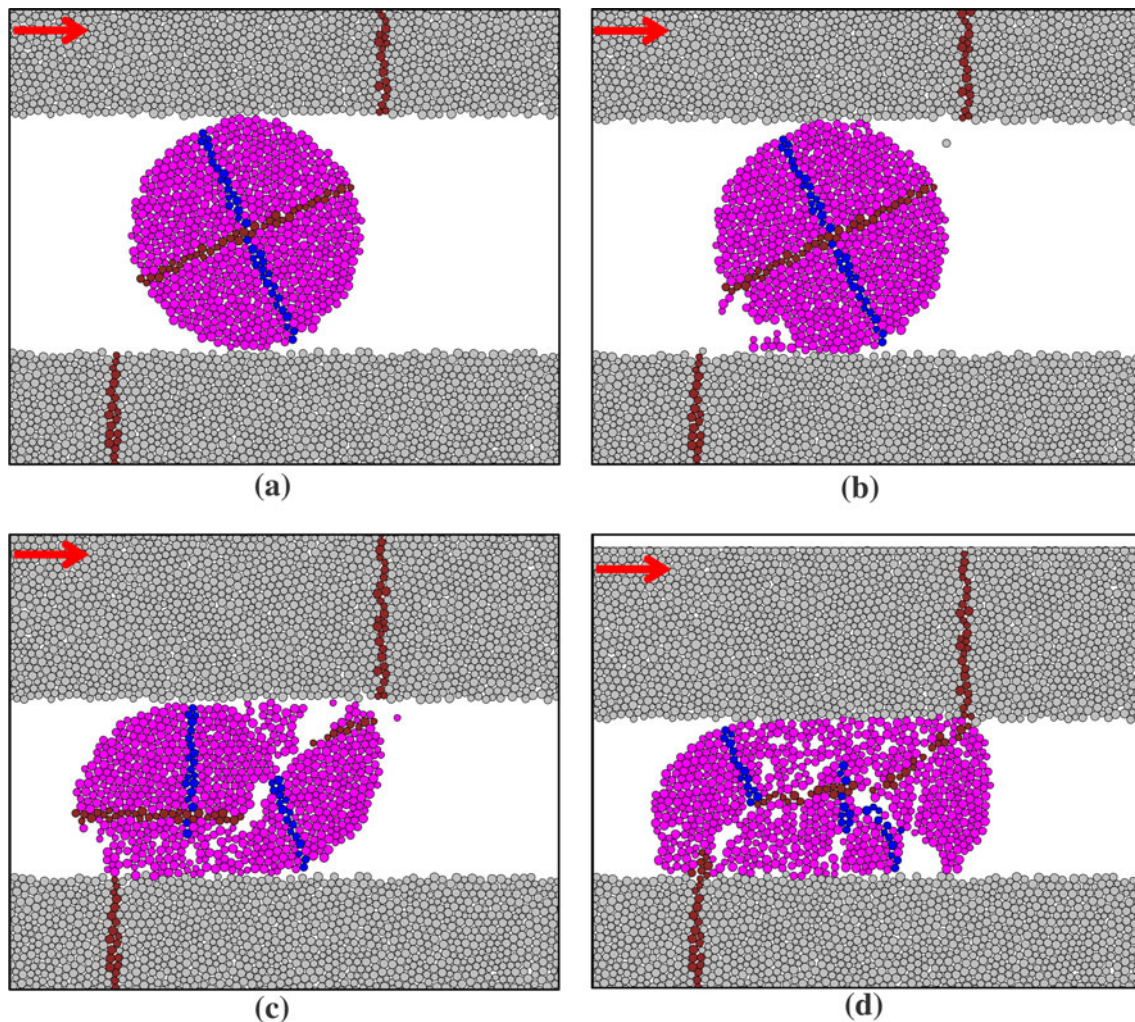


Fig. 2 Evolution of a single gouge particle in a rock fracture segment after a shear displacement of about 1.2 mm. Hereafter, the *red arrows* indicate that the upper wall moved in the right direction horizontally. **a** $\sigma_v = 0.225 \text{ MPa}$; **b** $\sigma_v = 0.5 \text{ MPa}$; **c** $\sigma_v = 0.75 \text{ MPa}$; **d** $\sigma_v = 1.0 \text{ MPa}$ (color figure online)

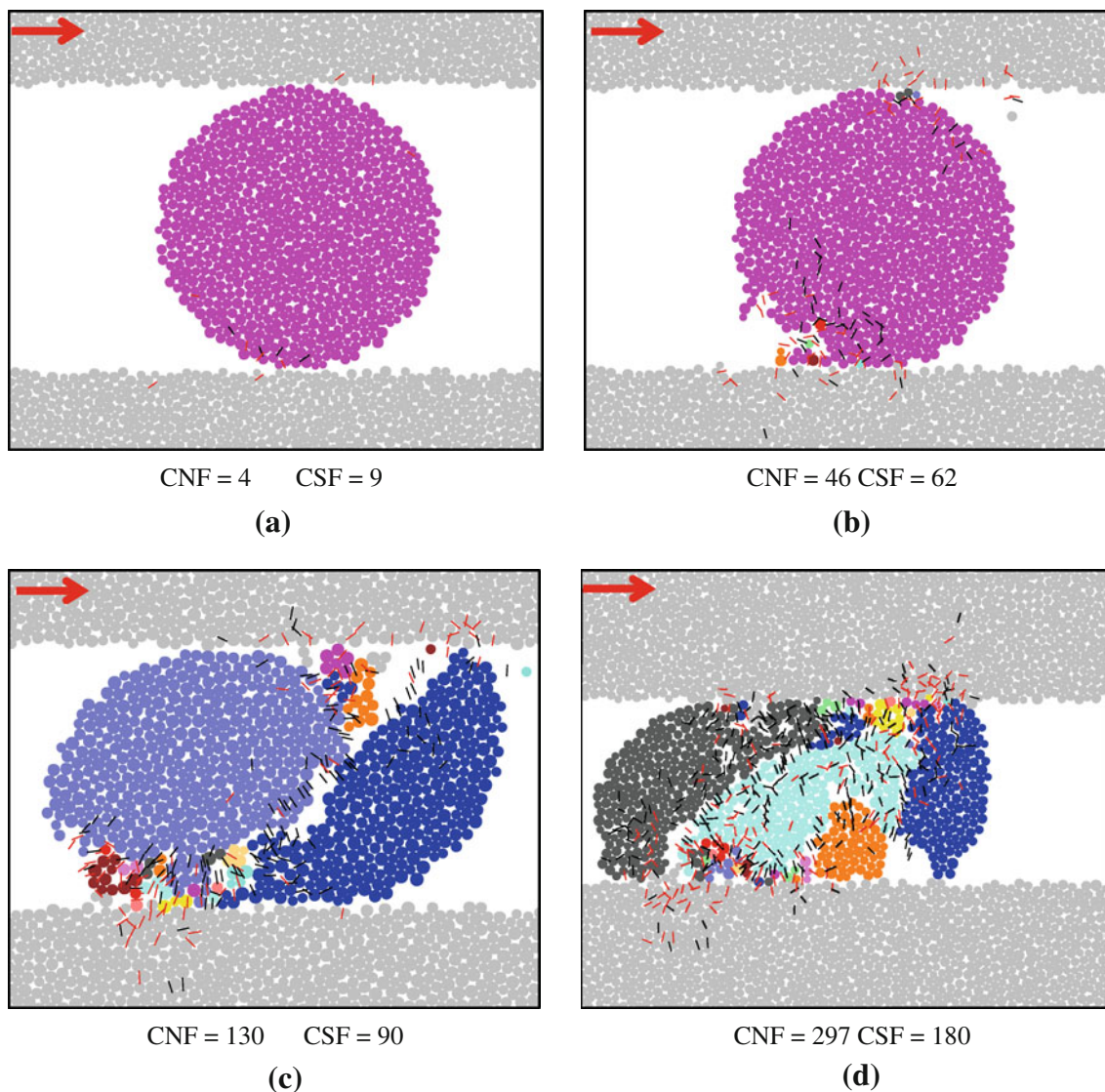


Fig. 3 The shape of crushed gouge particles after a shear displacement of about 1.2 mm for single gouge particle model. *Gray particles* represent fracture walls, and *other colors* represent crushed gouge particles. Microcracks generated in gouge particles and fracture walls are also indicated (*black and red short line segments* represent the

0.75 and 1.0 MPa, respectively, with many other smaller abrasive or comminuted particles (Fig. 3c, d). Figure 6 shows the sieve analysis of crushed gouge pieces under four different stress conditions. With increasing normal stress, the number of crushed gouge pieces increased significantly, induced by a large contact interface area between gouge particle and fracture walls, but the volume of large crushed pieces decreased.

3.1.2 Fracture Wall Behavior

With increasing normal stress, more microcracks developed in the shallow layers [damage zone defined by Zhao et al. (2012)] of fracture walls (Fig. 3), and more abrasive

tensile and shear cracks, respectively). CNF and CSF are the total number of tension and shear microcracks, respectively. **a** CNF = 10, CSF = 14, $\sigma_v = 0.225$ MPa; **b** CNF = 39, CSF = 57, $\sigma_v = 0.5$ MPa; **c** CNF = 145, CSF = 117, $\sigma_v = 0.75$ MPa; **d** CNF = 373, CSF = 215, $\sigma_v = 1.0$ MPa (color figure online)

particles were plowed off from the asperities of fracture walls (Table 2). The dominant damage in the shallow layer of the fracture wall was shear microcracks. Much more abrasive particles were generated from the upper wall under a normal stress of 1.0 MPa because it was moving. Under normal stresses of 0.225 and 0.5 MPa, a small magnitude of dilation was induced by the rolling of gouge particles (Fig. 7). Therefore, the roughness of both the fracture walls and gouge particle surface can result in dilation during the rolling process, and this could be another factor (in addition to the asperities sliding) contributing to the shear dilation that commonly occurred in the direct shear test. When normal stresses of 0.75 and 1.0 MPa were applied, fracture aperture gently closed

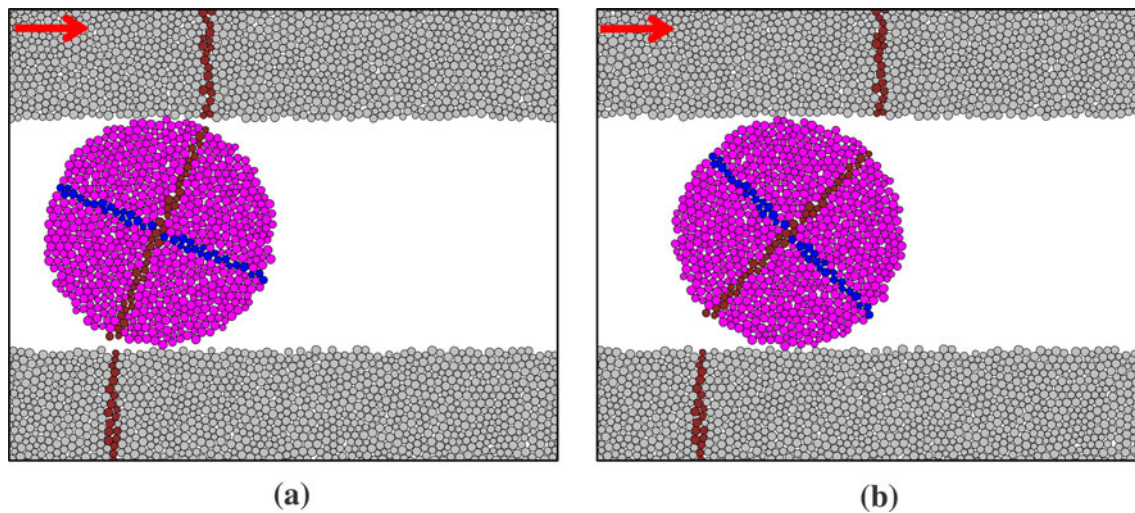


Fig. 4 Gouge particle rolling process under normal stress of 0.225 MPa for the single gouge particle model. **a** Shear displacement of 0.4 mm. **b** Shear displacement of 0.8 mm

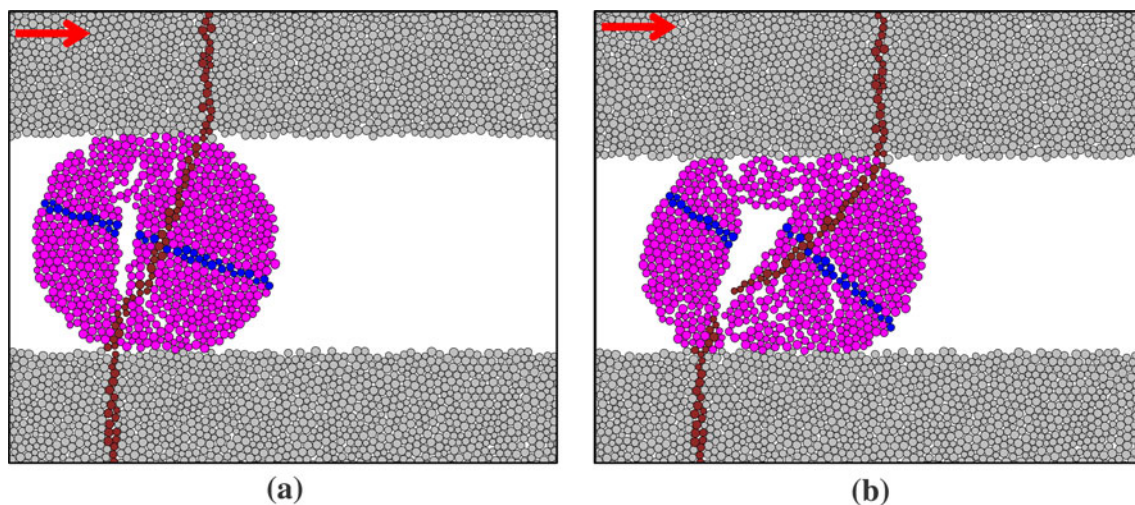


Fig. 5 Gouge particle rolling process under normal stress of 1.0 MPa for single gouge particle model. **a** Shear displacement of 0.4 mm. **b** Shear displacement of 0.8 mm

during the initial period (shear displacement < 0.4 mm) (Fig. 7). This resulted from surface erosion, but gouge particle rolling was still the dominant pattern of movement. With further shear, fracture aperture closure became more drastic because of the occurrence of gouge particle breakage, so the main type of gouge evolution changed from rolling into comminuting.

For the shear stress applied on the upper shear box (Fig. 7), there was an initial fluctuation under normal stress of 0.225 MPa, but after that the shear stress kept nearly constant. Besides the similar fluctuation of shear stress under a normal stress of 0.5 MPa, there were also a few peaks of shear stress in order to overcome the friction between fracture walls and gouge particles and keep the gouge particle rolling. Meanwhile, the damage developed

in the gouge particle and fracture walls. However, for the cases with normal stresses of 0.75 and 1.0 MPa, gouge breakage occurred continuously during the whole course, so the shear stress kept fluctuating (Fig. 7).

3.2 Two-Gouge Particles Model

3.2.1 Gouge Behavior

Initially, the two gouge particles were in contact with each other (Fig. 1b), but they separated during the shear process (Fig. 8a, b) under normal stresses of 0.225 and 0.5 MPa. The values for the horizontal displacements of left and right gouge centers were 0.09 and 0.56 mm, respectively, under a normal stress of 0.225 MPa. The distance that the

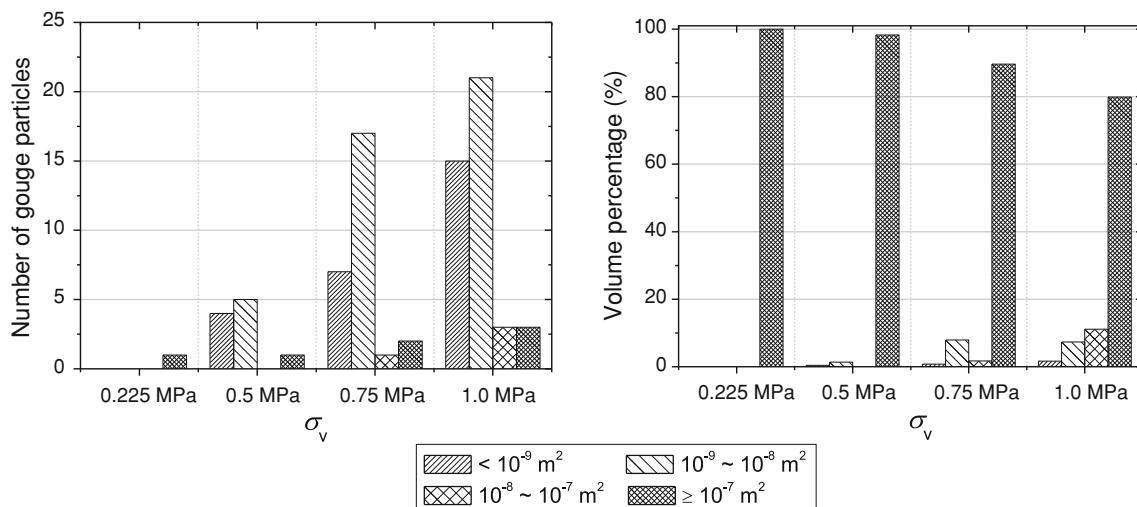


Fig. 6 Crushed piece size distribution after a shear displacement of about 1.2 mm for single gouge particle model

Table 2 Number of abrasive particles plowed from the fracture walls after a shear displacement of about 1.2 mm

Vertical stress (MPa)	Single-gouge particle model		Two-gouge particle model	
	Upper wall	Down wall	Upper wall	Down wall
0.225	0	1	0	0
0.5	2	3	1	1
0.75	2	3	0	3
1.0	8	3	14	6

right gouge particle moved was the same as that in the single gouge model. This is because the fracture surfaces were rough instead of smooth, and the gouge shapes were not perfect circles either. Therefore, during the shear process, the left gouge particle lost contact with the upper wall and stopped moving sometimes (Fig. 10). In contrast, the right gouge particle was in contact with the upper wall the

whole time, so the right gouge particle rolled much further than the left one (Fig. 8a, b). The minor surface erosion along the upper wall and inside the gouge particles could be monitored (Fig. 9a, b). Under normal stresses of 0.75 and 1.0 MPa, both gouge particles moved in a similar pattern (Fig. 8c, d), because they were fully in contact with fracture walls under large compression. The surface erosion also became much more severe (Fig. 9c, d), since the gouge particles must overcome stronger friction to move under larger normal stress. Note that some surface erosion was induced by the relative friction at the contacts of both gouge particles. Under a normal stress of 1.0 MPa, both gouge particles were almost broken into two major pieces, with only a small number of bonds left. Compared with the damage for the single gouge case (Fig. 5), the more severe microcracking and surface erosion occurred relatively late for two gouge particles under the same normal stress of 1.0 MPa. Figure 12 presents the sieve analysis of crushed gouge pieces with increasing normal stresses. Generally

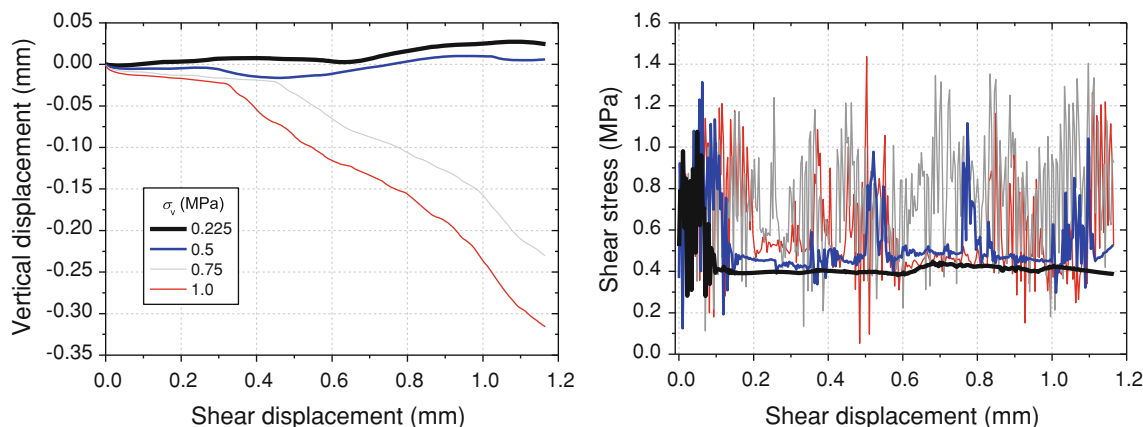


Fig. 7 Vertical displacement and shear stress versus shear displacement for the single gouge particle model

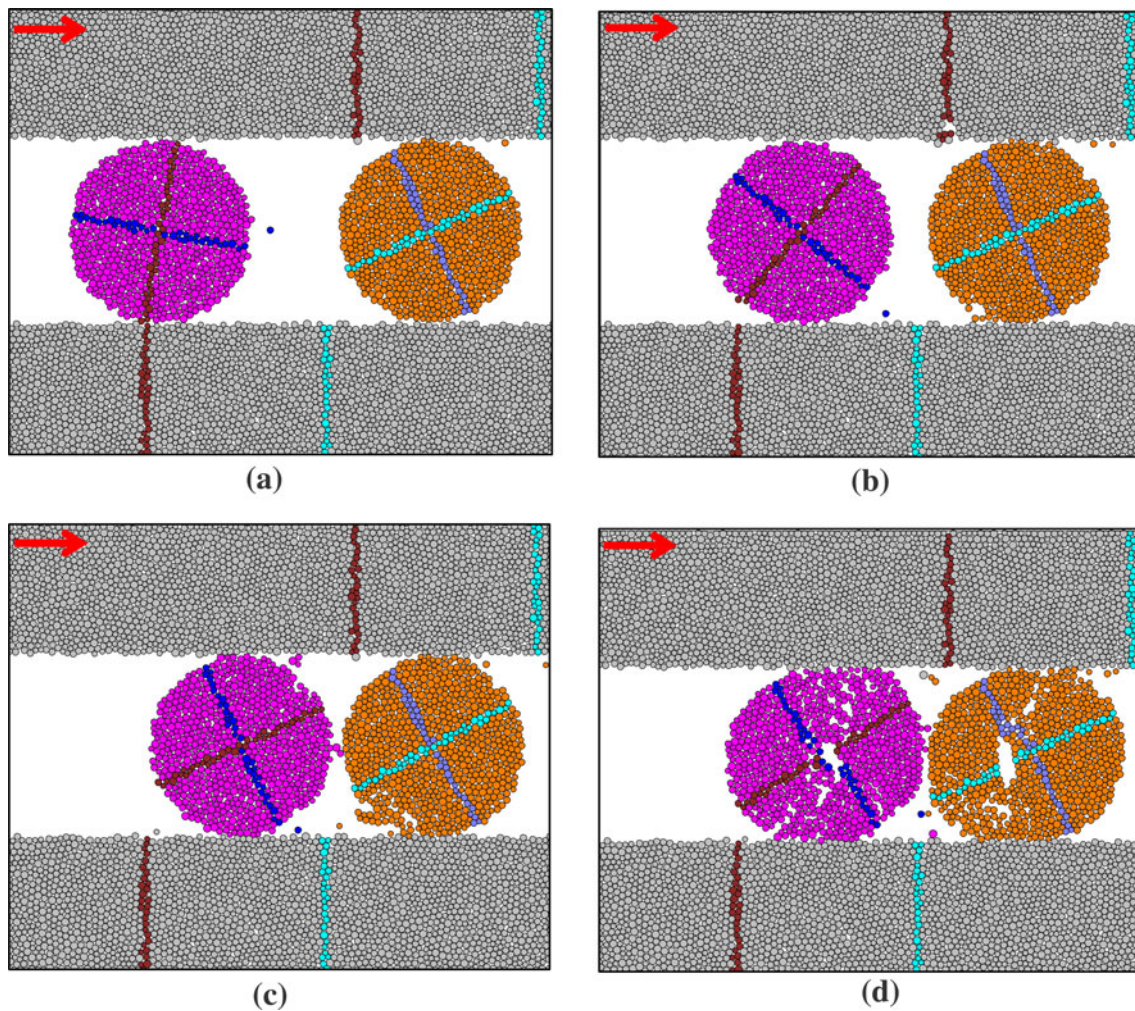


Fig. 8 Evolution of two contacted gouge particles in a rock fracture segment after a shear displacement of about 1.2 mm. **a** $\sigma_v = 0.225$ MPa; **b** $\sigma_v = 0.5$ MPa; **c** $\sigma_v = 0.75$ MPa; **d** $\sigma_v = 1.0$ MPa

speaking, more small pieces were plowed off from gouge particles with increasing normal stress after the same shear displacement, but the right gouge particle was damaged more seriously than the left one. This indicates that the gouge shape and roughness of the fracture surface also influence the gouge evolution. Even though under a normal stress of 1.0 MPa neither gouge particle was fully broken like in the single gouge case, if the shear process continued, full breakage would occur gradually.

3.2.2 Fracture Wall Behavior

As normal stress increased, more microcracks developed in the shallow zones of fracture surfaces (Fig. 9). The number of abrasive particles plowed off from fracture surfaces also increased (Table 2). Fracture dilation was monitored during the shear process under normal stresses of 0.225, 0.5 and 0.75 MPa, but the dilations were not constant during the shear process (Fig. 13). Under a

normal stress of 1.0 MPa, the fracture aperture started to decrease drastically after the shear displacement of about 0.9 mm. For the shear stress, initial fluctuations also exhibited under normal stresses of 0.225 and 0.5 MPa, after which it was almost stable, but with one or more peaks. The shear stress exhibited fluctuations during the whole shear process with normal stresses of 0.75 and 1.0 MPa applied. Overall, higher shear stresses are required to push the upper wall to move as normal stress increased (Fig. 13).

3.3 Main Differences Between the Above Two Cases

When two gouge particles exist in a fracture segment simultaneously, the normal stress applied to each of them was lower than that of only one gouge particle under the same normal stresses applied on the upper box. Therefore, all the damage, including microcracks, surface erosion and breakage, was less significant for the case of two gouge

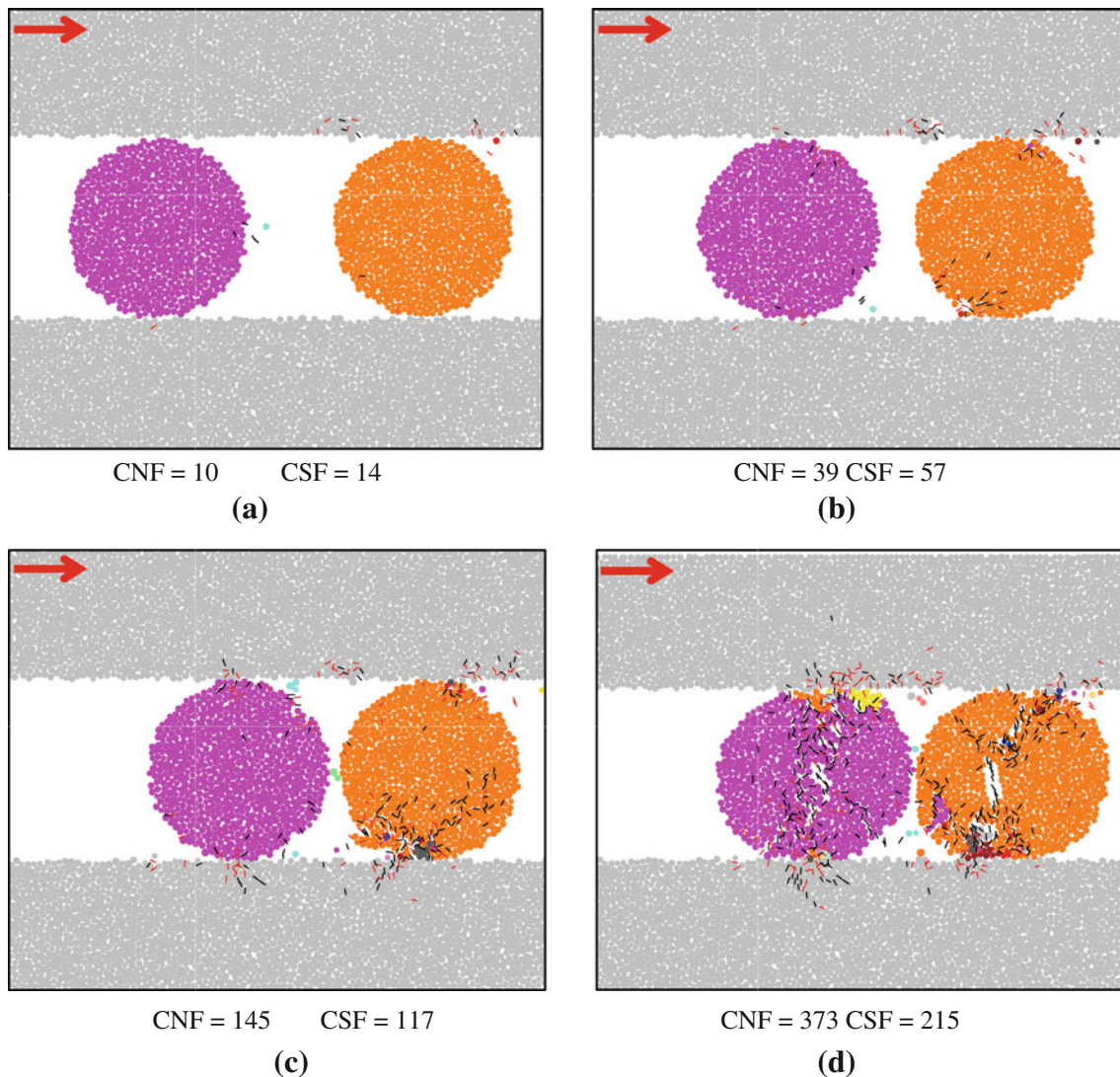


Fig. 9 The shape of crushed gouge particles after a shear displacement of about 1.2 mm for the two-gouge particle model. *Gray particles* represent fracture walls, and *other colors* represent crushed gouge particles. Microcracks generated in gouge particles and fracture walls are also indicated (*black and red short line segments* represent

the tensile and shear cracks, respectively). **a** CNF = 10, CSF = 14, $\sigma_v = 0.225$ MPa; **b** CNF = 39, CSF = 57, $\sigma_v = 0.5$ MPa; **c** CNF = 145, CSF = 117, $\sigma_v = 0.75$ MPa; **d** CNF = 373, CSF = 215, $\sigma_v = 1.0$ MPa (color figure online)

particles, and the occurrence of damage was also delayed. During the shear process, one of the two gouge particles could lose contact with the moving fracture wall under low normal stress; thus, it became similar to the single gouge case where only one gouge particle rolled with the moving fracture wall. This can partly explain the persistence of survivor gouge particles (defined as particles that retain 75 % of their original size) in a sheared fracture filled in with a large number of gouge particles (Mair and Abe 2008). Another obvious distinction is the interaction between gouge particles that could induce surface erosion (plowed pieces) at the interfaces between two gouge particles.

4 Microparameter Sensitivity Analysis

In general, the particle mechanics model is characterized by the microparameters listed in Table 1, each of which may influence the macroscopic model behaviors (Potyondy and Cundall 2004). Therefore, synthetic biaxial, Brazilian and direct shear tests are commonly used to calibrate these microparameters in order to reasonably represent the basic mechanical properties of intact rocks and rock joints (Wang et al. 2003; Potyondy and Cundall 2004; Asadi et al. 2012). Even though the microparameters used in Sect. 3 were demonstrated to be proper for rocks like granite, sensitivity analysis was still carried out in this section to

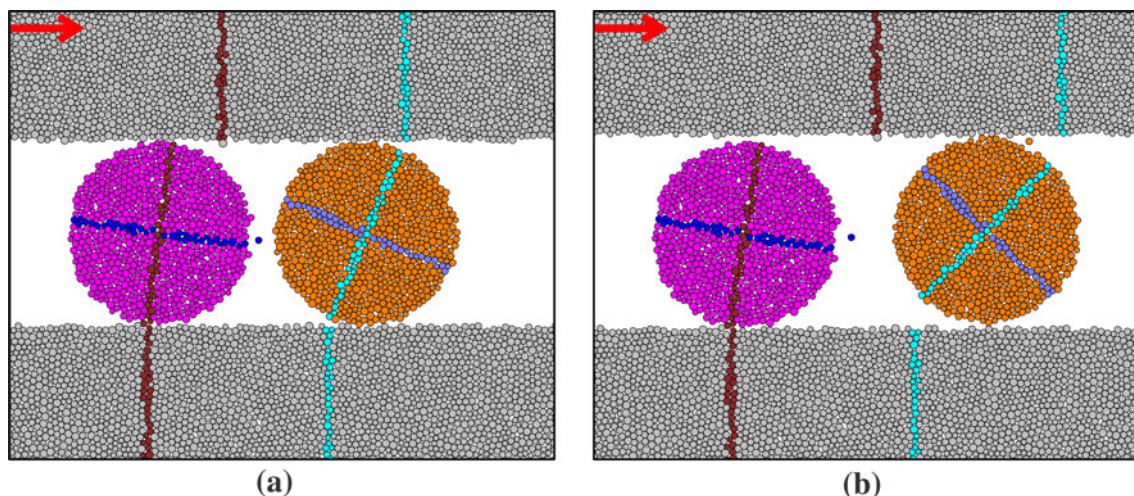


Fig. 10 Gouge particle rolling process under normal stress of 0.225 MPa for two-gouge particle model. **a** Shear displacement of 0.4 mm. **b** Shear displacement of 0.8 mm

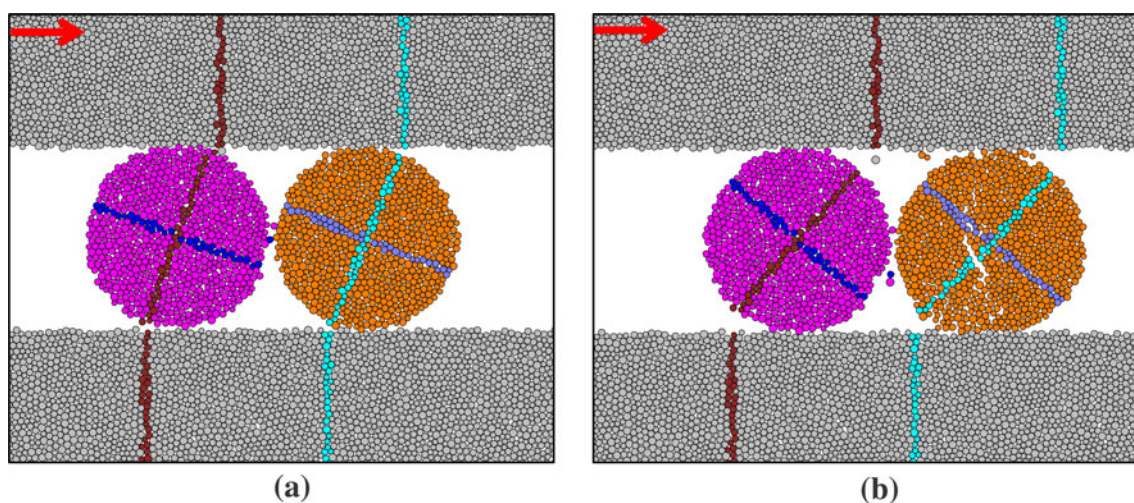


Fig. 11 Gouge particle rolling process under normal stress of 1.0 MPa for the two-gouge particle model. **a** Shear displacement of 0.4 mm. **b** Shear displacement of 0.8 mm

investigate the influences of microparameters in a generic study. The effects of ball size, contact friction coefficient, mean strength and contact modulus on the gouge evolution were investigated, respectively. For the sensitivity analysis, the models using the microparameters in the middle column of Table 1 were used as reference, and the values of the investigated items were varied correspondingly (in the right column of Table 1) for comparison. All the models were run 310,000 time steps after the shear started under the normal stresses of 0.225 and 1.0 MPa, respectively. In this way, the effects of microparameters on the two different types of gouge evolution can be studied, without losing generality. The analysis concentrated on single gouge particle cases in this section for simplicity.

4.1 Effect of Average Ball Size

Four PFC models were built using the microparameters in Table 1, but including different numbers of balls, 5,000, 10,000, 15,000 and 20,000, respectively. The average radius of balls for these four models was 2.93×10^{-2} , 2.07×10^{-2} , 1.70×10^{-2} and 1.47×10^{-2} mm, respectively. A smaller number of balls in the model induced larger time steps, so the shear displacements of the upper walls were 2.03, 1.43, 1.17 and 1.01 mm after 310,000 time steps, respectively. Under normal stress of 0.225 MPa, the dominant pattern of gouge particle movement was rolling regardless of the average ball sizes, but the horizontal displacements of gouge center were 1.02, 0.74, 0.56 and

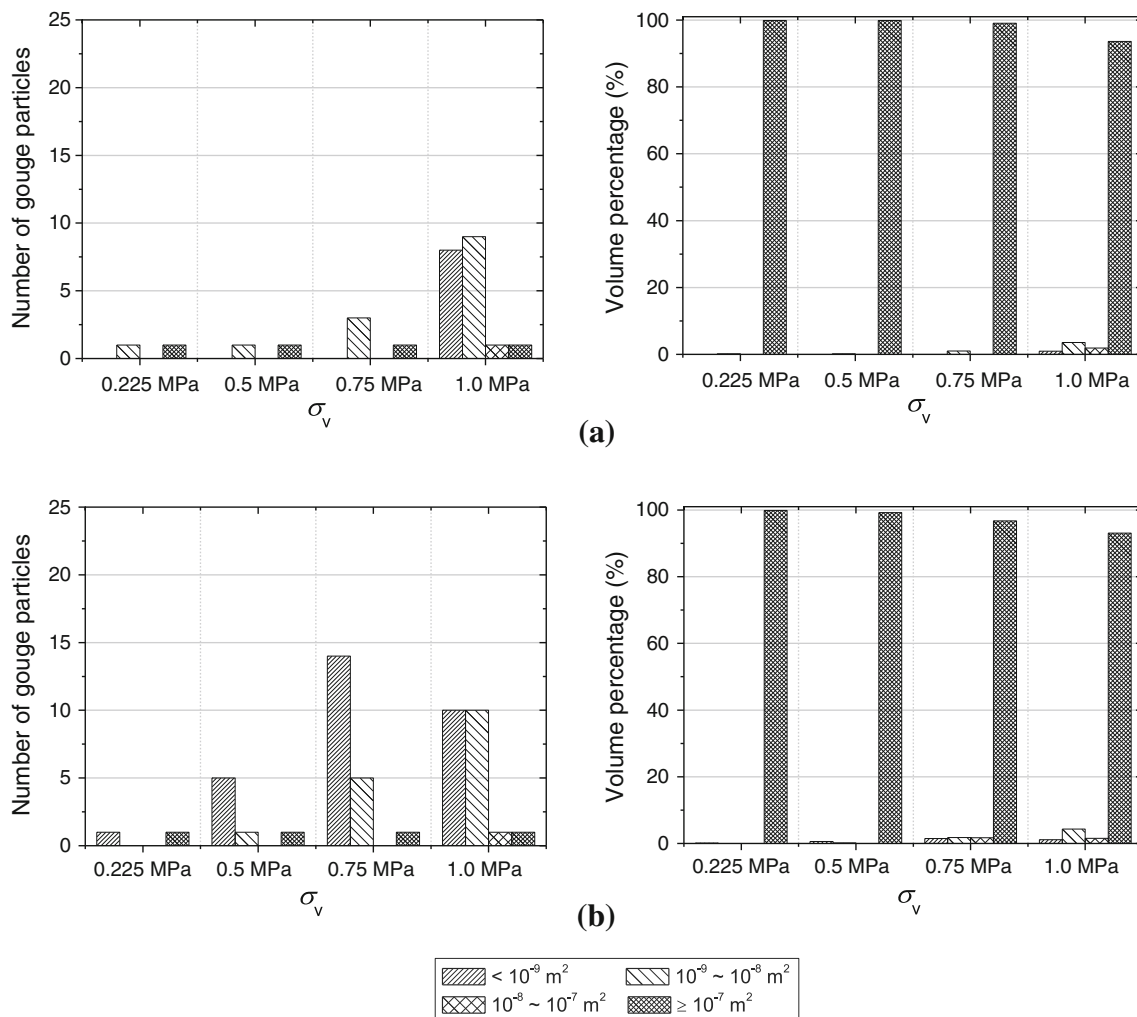


Fig. 12 Crushed piece size distribution after a shear displacement of about 1.2 mm for the two-gouge particle model. **a** Gouge 1. **b** Gouge 2

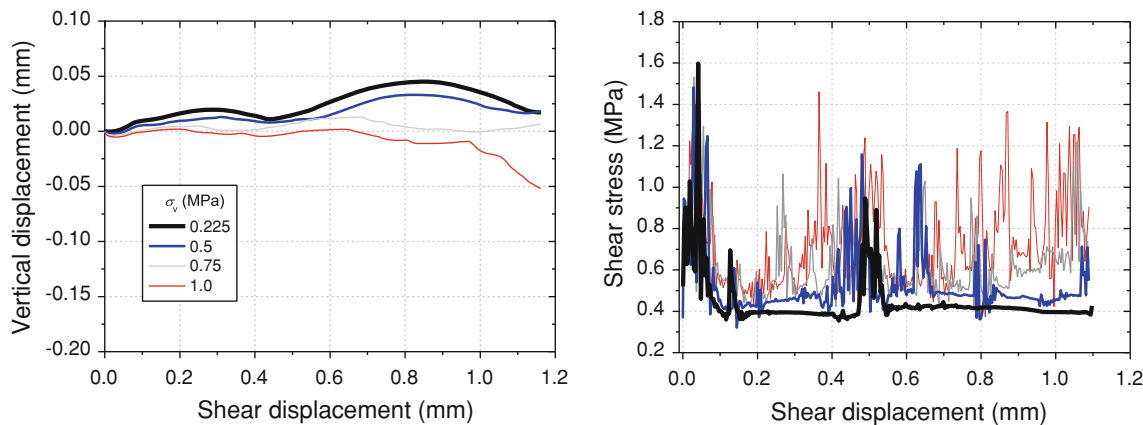


Fig. 13 Vertical displacement and shear stress versus shear displacement for the two-gouge particle model

0.50 mm, respectively. The rolling angles were about 108°, 80°, 65° and 54° with decreasing ball size, and the arc lengths of the rolling gouge particles can be calculated as

approximately 1.88, 1.40, 1.13 and 0.94 mm, respectively. Compared with the shear displacements of upper walls, the values of arc lengths of rolling gouge particles were a little

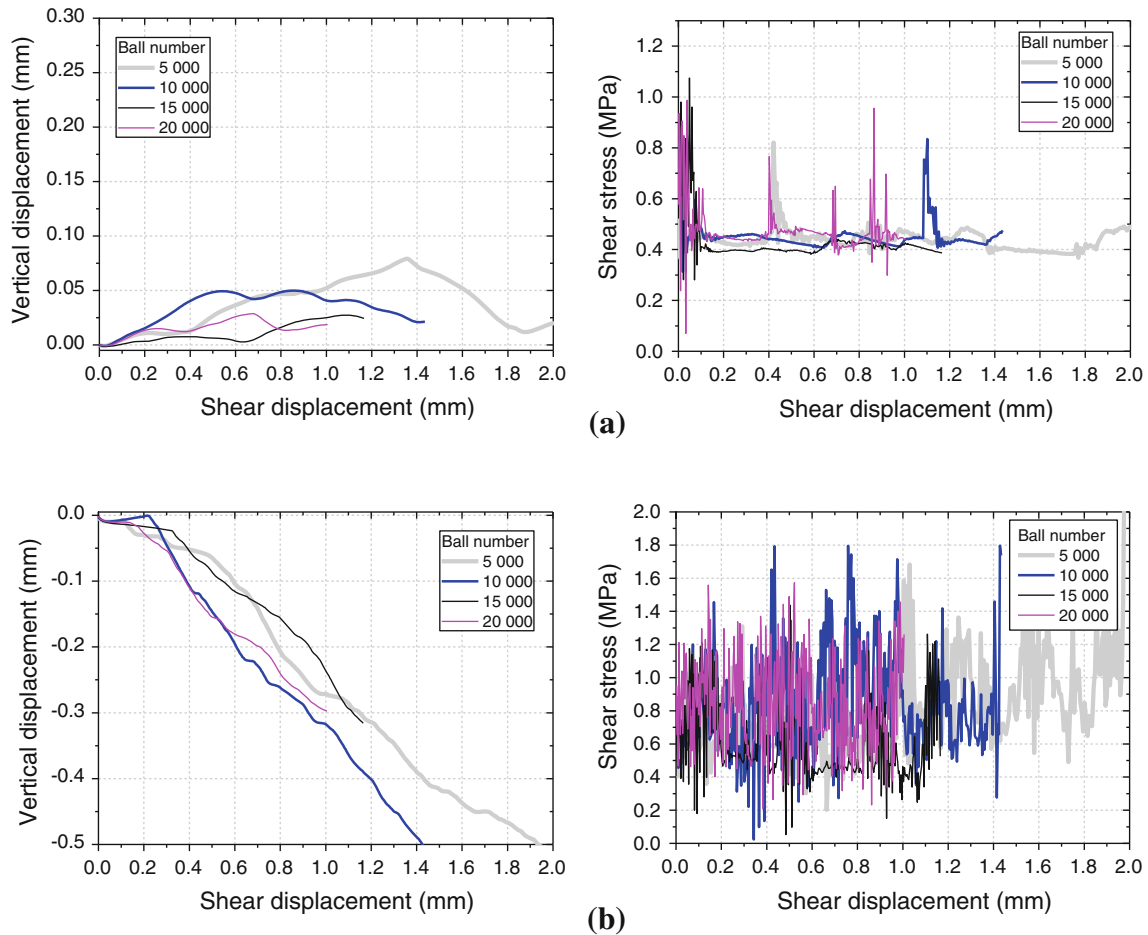


Fig. 14 Comparison of fracture specimens with varying ball numbers (i.e., average radius) after 310,000 time steps. **a** Normal stress of 0.225 MPa. **b** Normal stress of 1.0 MPa

small. This indicates that the pure sliding of the fracture wall without gouge rolling occurred for some short moments, especially for the models of coarse resolution. The development of very few microcracks and none of the abrasive particles suggests that surface erosion was negligible for all models. The fracture apertures started to re-open after a slight closure after shear started (Fig. 14a). After the first peak of shear dilation, the magnitude of dilation changed with further shear displacement, but fracture apertures kept

the states of dilation (larger aperture than the initial state) the whole time. Ball sizes changed packing arrangements and consequently changed the shear dilation-shear displacement curve. However, the shear stresses required to cause the gouge particle rolling were similar (around 0.4 MPa) in spite of varying ball sizes (Fig. 14a).

When normal stress of 1.0 MPa was applied, four gouge particles were crushed into a large number of small pieces (Table 3). For models of relatively coarse resolution

Table 3 Comparison of fracture specimens with varying ball numbers (i.e., average radius) after a shear displacement of about 1.2 mm under a normal stress of 1.0 MPa

Ball number	Mean radius (mm)	Number of abrasive particles from walls		Size distribution of crushed gouge pieces (volume %)			
		Upper wall	Down wall	$<10^{-9} \text{ m}^2$	$10^{-9}-10^{-8} \text{ m}^2$	$10^{-8}-10^{-7} \text{ m}^2$	$\geq 10^{-7} \text{ m}^2$
5000	2.93×10^{-2}	5	2	0.00 %	20.32 %	63.76 %	15.92 %
10000	2.07×10^{-2}	3	0	0.42 %	19.55 %	32.42 %	47.61 %
15000	1.70×10^{-2}	8	3	1.63 %	7.36 %	11.11 %	79.90 %
20000	1.47×10^{-2}	15	5	2.04 %	9.57 %	17.85 %	70.40 %

(average ball radius 2.93×10^{-2} and 2.07×10^{-2} mm), many more fine gouge pieces ($<10^{-8}$ m²) were generated. More abrasive balls were plowed off from the upper wall for all the models, and models with an average ball radius of 2.07×10^{-2} and 1.47×10^{-2} mm generated the least and most abrasive balls, respectively. However, the coarsest model produced the largest volume (2.38×10^{-8} m²) of abrasive balls from fracture walls, and the volumes of abrasive balls for the other three models were 3.27×10^{-9} , 9.99×10^{-9} and 1.01×10^{-8} m², respectively, with decreasing ball size. This also indicates that the different outer waviness of gouge particles due to different packing arrangements influenced the gouge evolution and surface damage. Figure 14b shows the fracture closure with shear displacement, which exhibits that the model of an average ball radius of 2.07×10^{-2} mm had the largest aperture closure. The drastically fluctuating shear stresses with shear displacements are also shown in Fig. 14b.

4.2 Effect of the Friction Coefficient

With changing friction coefficient from 0.4 to 0.8 by an interval of 0.1, five models with other microparameters in the middle column of Table 1 were tested. In addition, a model of a relatively small friction coefficient 0.05 was also run for comparison (Table 4; Fig. 15). The friction coefficient did not change time steps in any of the calculations, so all five fracture segments were sheared by about 1.17 mm after 310,000 time steps. Under a normal stress of 0.225 MPa, the horizontal displacements of gouge centers were about 0.55 mm for the model with a friction coefficient of 0.4, but other gouges moved horizontally at a distance of about 0.56 mm. This means that the gouge particles moved in the way of pure rolling, so the shear stress remained stable after the steady states of rolling were achieved (Fig. 15a). The shear dilation curves almost overlap each other except the models with friction coefficients of 0.05 and 0.4. Instead of rolling, the upper wall sliding over the gouge particle might occur under this condition. This could be the reason why the gouge particle

in the model of friction coefficient 0.4 moved the shortest distance. The rolling of the gouge particle would then restart when more contacts between upper wall and gouge re-formed with shear displacement. This is why the shear stress had more fluctuations for the models of friction coefficients 0.05 and 0.4 after shear stress became stable.

If normal stress increased to 1.0 MPa, the effects of the friction coefficient became significant. Generally with increasing friction coefficients, more gouge pieces of small sizes were generated, and more abrasive balls were plowed after a shear displacement of 1.17 mm (Table 4). Fracture closure occurred for all the models, and models with friction coefficients of 0.05 and 0.4 had larger aperture closures, but the model of friction coefficient 0.6 yielded the smallest closure. This indicates that the behaviors of gouge particles became more complex after breakage occurred. The shear stress fluctuated significantly for all six models during the whole shear process.

4.3 Effect of Strengths

The mean normal and shear strengths of contact bonds between balls varied from 10, 20 to 30 MPa in order to examine the effects of contact bond strengths on gouge evolution. It was assumed that both normal and shear strengths have the same values. Contact bond strengths did not change the time step in calculations, so the shear displacements of the upper box were about 1.17 mm after 310,000 time steps. For the models of mean strengths of 20 and 30 MPa, they exhibited similar behaviors of gouge evolution under normal stress of 0.225 MPa. The gouge particle moved at a distance of 0.56 mm in the shear direction, without the occurrence of significant surface erosion on fracture walls and gouge surfaces. The shear dilation for these two models also varied in the same way, and the stable shear stresses were about 0.4 MPa. Due to the small strengths in the model of mean strengths of 10 MPa, about 1.5 % of gouge volume was eroded from the original gouge particle, and the fracture aperture

Table 4 Comparison of fracture specimens with varying friction coefficients after a shear displacement of about 1.2 mm under a normal stress of 1.0 MPa

Friction coefficient	Number of abrasive particles from walls		Size distribution of crushed gouge pieces (volume %)			
	Upper wall	Down wall	$<10^{-9}$ m ²	10^{-9} – 10^{-8} m ²	10^{-8} – 10^{-7} m ²	$\geq 10^{-7}$ m ²
0.05	3	0	0.44 %	7.53 %	1.64 %	90.39 %
0.4	4	2	1.14 %	13.15 %	19.70 %	66.01 %
0.5	5	5	1.58 %	10.02 %	10.42 %	77.97 %
0.6	8	3	1.63 %	7.36 %	11.11 %	79.90 %
0.7	14	4	2.04 %	13.78 %	10.23 %	73.95 %
0.8	20	6	2.36 %	9.73 %	4.75 %	83.15 %

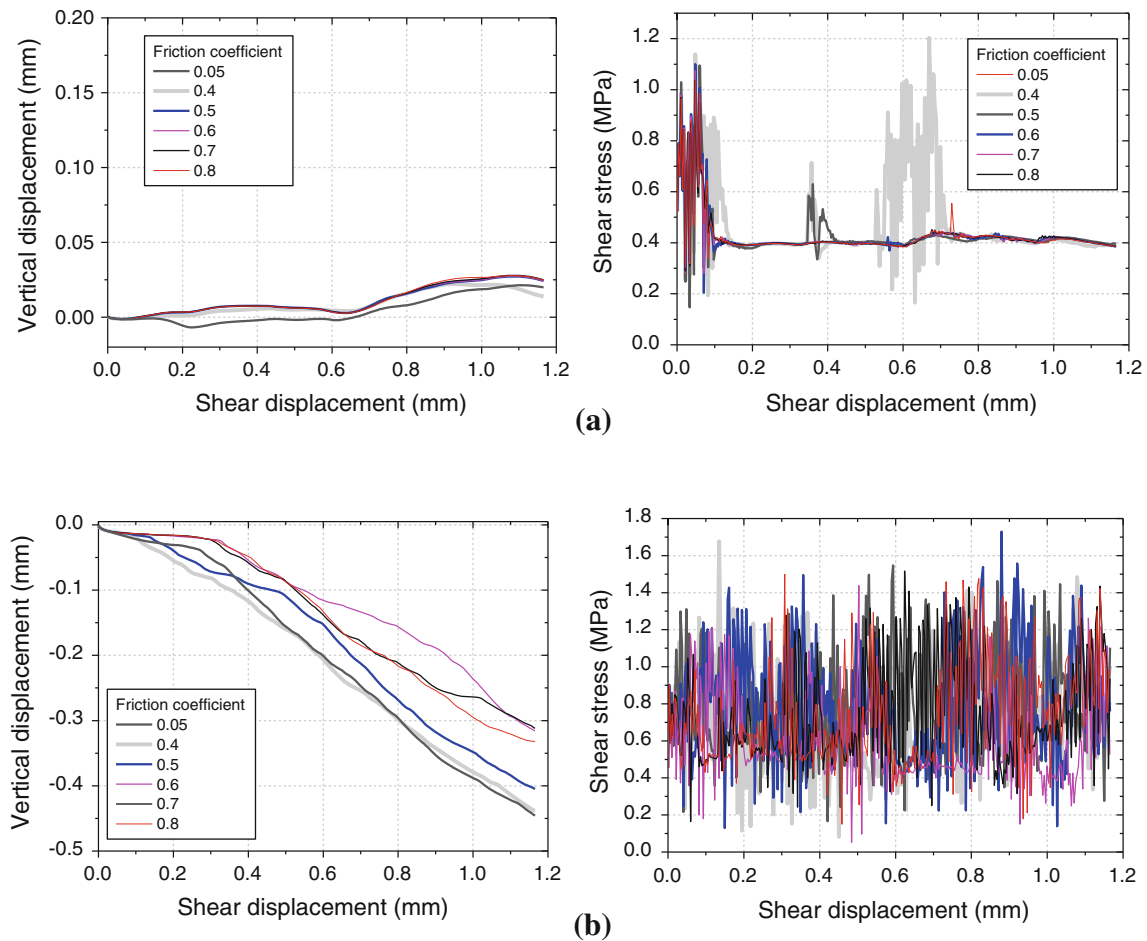


Fig. 15 Comparison of fracture specimens with varying ball–ball friction coefficients after 310,000 time steps. **a** Normal stress of 0.225 MPa. **b** Normal stress of 1.0 MPa

continuously closed instead of re-opening. The shear stress was also oscillated to keep the upper box moving at a steady velocity. Fracture surface erosion also occurred, and a total of 14 and 1 abrasive balls were cut from upper and lower fracture walls.

With normal stress of 1.0 MPa applied, three gouge particles were fully broken, but the difference is that the original gouge particle was comminuted into a large number of small pieces for the weakest model, i.e., the pieces with size $<10^{-8} \text{ m}^2$ took up about 50 % of the original gouge volume (Table 5). For the other two models, more gouge pieces of large sizes ($>10^{-7} \text{ m}^2$) existed. Similarly, with decreasing mean strengths, more abrasive balls were plowed from fracture walls (Table 5). Because larger interfaces between gouges and fracture walls were induced by the severe damage in the model of 10 MPa mean strengths, the shear stress was larger than that for the other two models so as to overcome the stronger friction

(Fig. 16). Larger mean strengths were also beneficial to resist the fracture closure and surface erosion.

4.4 Effect of the Contact Modulus

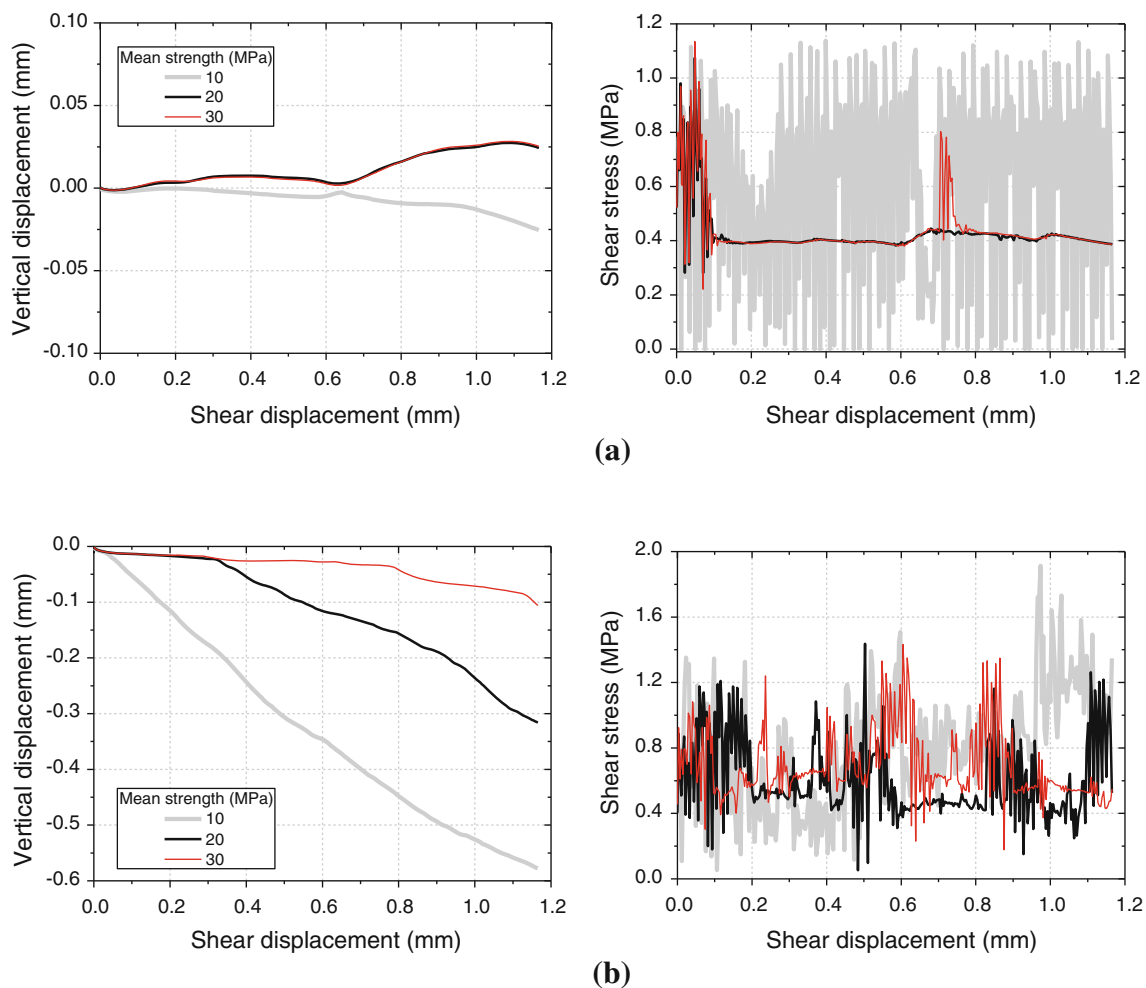
The contact modulus not only determines the deformability of ball contacts, but also controls the size of time steps (Itasca Consulting Group Inc 2008). A larger contact modulus results in a smaller time step, and the relationship between the contact modulus and (normal and shear) stiffness of contacts between balls can be found in Potyondy and Cundall (2004). The contact modulus was varied from 0.5, 5.0 to 50.0 GPa to investigate its influences on gouge evolution. Due to the different magnitudes of time steps, the displacements for the three upper boxes were 3.70, 1.17 and 0.37 mm in the horizontal direction, but the horizontal displacements of three gouge particles were 1.79, 0.56 and 0.01 mm, respectively, under a normal

Table 5 Comparison of fracture specimens with varying mean strengths after a shear displacement of about 1.2 mm under normal stress of 1.0 MPa

Mean strength (Mpa)	Number of abrasive particles from walls		Size distribution of crushed gouge pieces (volume %)			
	Upper wall	Down wall	$<10^{-9} \text{ m}^2$	$10^{-9}-10^{-8} \text{ m}^2$	$10^{-8}-10^{-7} \text{ m}^2$	$\geq 10^{-7} \text{ m}^2$
10	29	4	5.10 %	43.30 %	32.21 %	19.38 %
20	8	3	1.63 %	7.36 %	11.11 %	79.90 %
30	1	1	0.48 %	4.34 %	3.78 %	91.41 %

stress of 0.225 MPa. In addition, the basic gouge evolution pattern did not change even when normal stress of 1.0 MPa was applied (Fig. 17). For the model with a contact modulus of 0.5 GPa, the gouge particle still kept rolling under normal stress of 1.0 MPa, without obvious surface erosion (Table 6), and the fracture aperture did not close that much compared with the condition of normal stress of 0.225 MPa. Because the dominant movement was rolling

without damage, the shear stress basically remained stable (Fig. 17). In contrast, the gouge particle in the model with a contact modulus of 50.0 GPa started to break up from the top point and almost stayed at the original position, regardless of the normal stresses. The surface erosion was also less significant compared with the model of the contact modulus of 5.0 GPa. This indicates that the contact modulus can play an important role in controlling the gouge

**Fig. 16** Comparison of fracture specimens with varying average strengths after 310,000 time steps. **a** Normal stress of 0.225 MPa. **b** Normal stress of 1.0 MPa

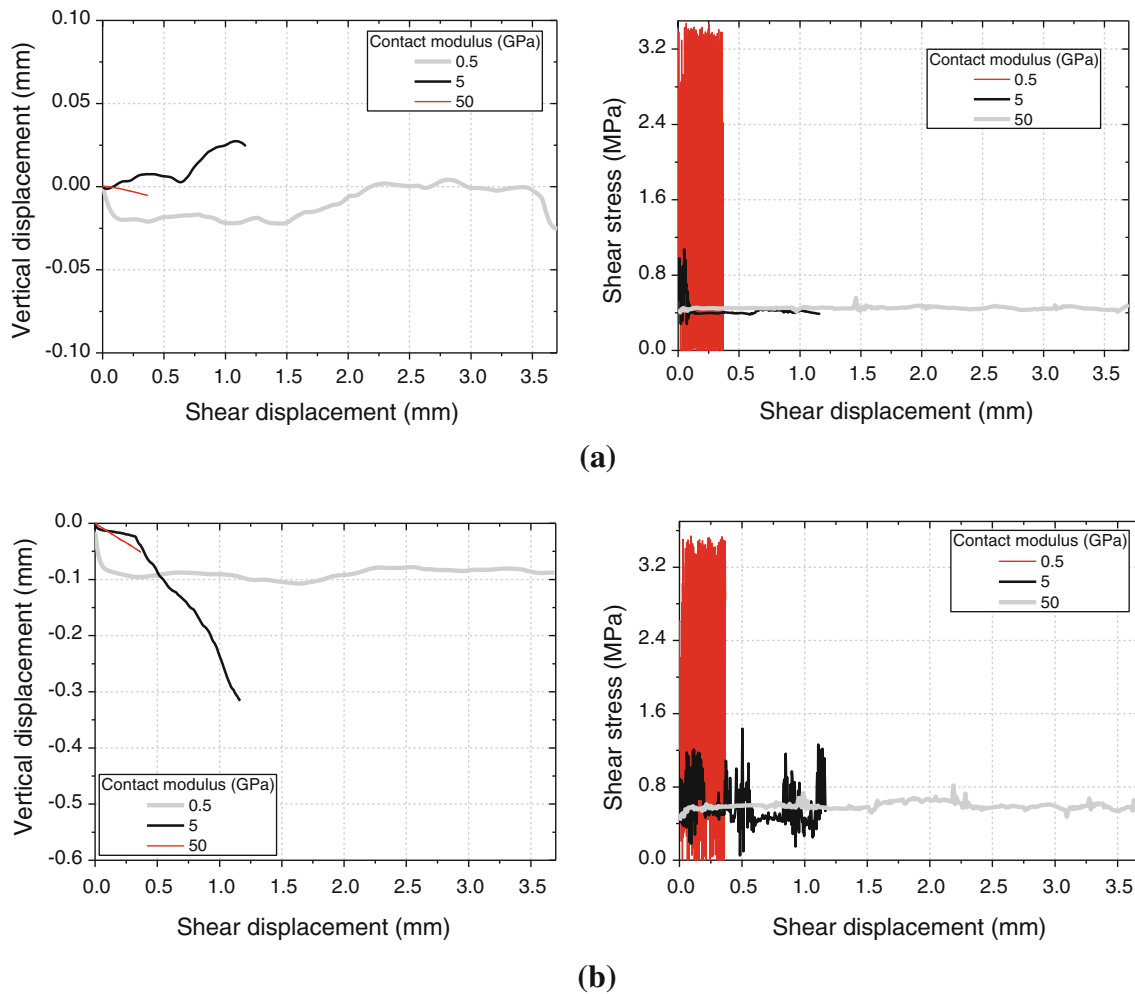


Fig. 17 Comparison of fracture specimens with varying contact moduli after 310,000 time steps. **a** Normal stress of 0.225 MPa. **b** Normal stress of 1.0 MPa

Table 6 Comparison of fracture specimens with varying contact moduli after a shear displacement of about 1.2 mm under a normal stress of 1.0 MPa

Contact modulus (GPa)	Number of abrasive particles from walls		Size distribution of crushed gouge pieces (volume %)			
	Upper wall	Down wall	$<10^{-9} \text{ m}^2$	$10^{-9}-10^{-8} \text{ m}^2$	$10^{-8}-10^{-7} \text{ m}^2$	$\geq 10^{-7} \text{ m}^2$
0.5	2	1	0 %	0 %	0 %	100 %
5	8	3	1.63 %	7.36 %	11.11 %	79.90 %
50	1	0	0.47 %	5.19 %	0 %	94.33 %

evolution in fractures, and values should be carefully calibrated in modeling attempts.

5 Discussions

5.1 Comparison with Experiments

The main novelty of this study was studying a short fracture segment containing gouge materials undergoing shear

rather than the whole fracture macroscopically. The results obtained from this microscopic modeling were in good agreement with other laboratory tests. Pereira and de Freitas (1993) divided the shear process into seven stages based on the observation of single fractures under ring shear. During the second stage of ‘mobilization of sliding,’ they found abrasion occurred by wearing the contact asperities, and this mechanism was successfully simulated with PFC in Zhao et al. (2012). As shear displacement continued, rolling friction eventually became dominant

when sufficient abrasive particles were generated from fracture walls to form a film of gouge (Pereira and de Freitas 1993). Similarly, the present modeling shows the gouge particles rolled with the moving upper fracture wall under low normal stress (Figs. 2, 4, 8, 10). Even under high normal stress, the gouge particles also rotated to some angle before breaking (Figs. 5, 11). Further shear displacement subjected the gouge particles to a significant crushing (Pereira and de Freitas 1993), which is also discovered in the present modeling under high normal stress (Figs. 3, 9). In addition, both the experiments and this modeling show that the gouge materials accumulated over the downstream part (Figs. 2, 8, 18). For the gouge particle under much higher normal stress of 5.0 MPa and after a long shear displacement of 2.0 mm, the original gouge particle was comminuted into a large number of tiny pieces, which formed a gouge film that almost filled the fracture voids (Fig. 18). The gouge film was also observed in the study of Pereira and de Freitas (1993). More tension microcracks in gouge particles indicated that the dominant failure mode within gouge particles was tension, because of the tension stress induced by normal loading. The tension strength of gouge particles was estimated at about 6.7 MPa with the Brazilian test, with the result that the gouge particle would not fail in the same fracture segment as long as the normal stress was lower than 1.6 MPa under pure compression. However, it was shown that the gouge particle failed under normal stress of 0.75 MPa, which indicates that the shear stress played an important role in the gouge failure. Many more shear microcracks in the fracture walls illustrate that the fracture surfaces were eroded in shear conditions (Pereira and de Freitas 1993). Generally, the modeling results can somehow clearly show the shear mechanisms in a rock fracture.

5.2 Implications for Macroscopic Fracture Behavior

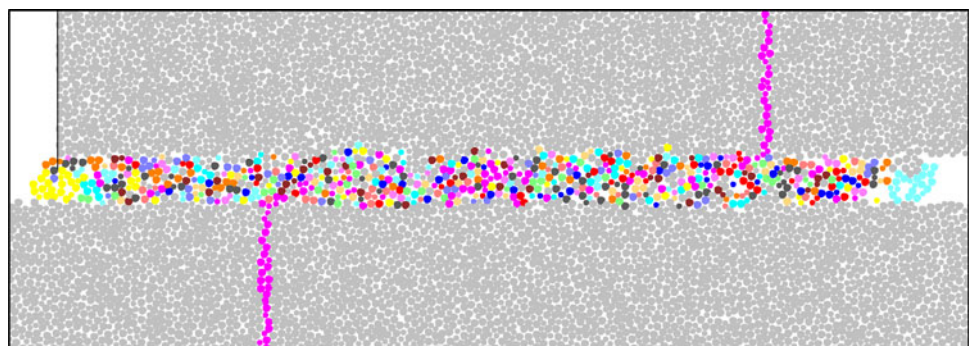
Even though this microscopic modeling cannot reflect the whole shear process, it provides some interpretations for the shear mechanisms occurring in a rock fracture. For a

clear fracture undergoing shear, abrasive gouge particles would be plowed from contacting asperities, and then the shear movement can change from surface sliding to gouge rolling. Consequently, it is predicated that the measured friction angle should decrease, which is demonstrated by the shear stress–shear displacement curve in Pereira and de Freitas (1993). Similarly, it was shown that rock fractures may exhibit smaller friction angles under higher normal stress; one possible reason is the generated abrasive particles (without failure) that may reduce the contact area between two fracture walls. Meanwhile, rolling is much easier than sliding. Further increasing normal stress would crush the gouge particles, so the shear stress also increases, but is still lower than the peak shear stress (the stage of second cycle of shearing). Generally, many experiments have shown that the infilling materials can significantly decrease the shear strength (e.g., Papaliangas et al. 1993; Pereira 1997; Boulon et al. 2002). The gouge particles contribute to this decreasing shear strength in terms of rolling and reducing sliding surfaces. According to the present results, it can also be expected that the hydraulic behavior of rock fractures is also influenced by gouge evolution. With shear displacement, the fracture aperture may increase or decrease under low or high normal stresses, respectively. Gouge particles may move or re-accumulate after breaking in the fracture voids, and this can change the possible (groundwater) flow pattern. Inversely, the gouge evolution may also be influenced by the fluid existing in or flowing through rock fractures.

5.3 Limitations

As a first-step attempt to investigate the gouge evolution in a short fracture segment, some simplifications were employed in this generic study. In this study, the profile of fracture segments was assumed to be a horizontal line, so it can only consider the fracture roughness by the arrangement of balls representing fracture walls. However, the actual fracture profile curves are of waviness, which may also change the gouge evolution and redistribution. In the

Fig. 18 The distribution (film) of crushed gouge particles after a shear displacement of 2 mm under a normal stress of 5.0 MPa. The two vertical magenta markers show the movement of upper wall



present models, the gouge particles were idealized (simplified) as circular discs, but in reality the shapes of gouge particles can be in any three-dimensional irregular shapes. The gouge particles with irregular shapes probably cannot roll perfectly like a circular disc, but they could fail in a similar pattern, as presented above. Actually, both rock fractures and gouge particles are three-dimensional, and three-dimensional modeling can be easily extended to consider the gouge behavior in the third dimension. In this study it was assumed that both fracture walls and gouge particles had the same properties, but there may be some differences between gouge materials and intact rocks due to the fact that the composition of gouge materials may not be pure rock minerals, but may include other materials like clay. In addition, gouge evolution may also be influenced by the water pressure or temperature field. Based on different gouge behaviors under various normal stresses, the normal loading conditions were classified as high and low normal stresses. Note that the thresholds of classification are actually dependent on the specific rock strength.

6 Conclusion

Gouge evolution in a rock fracture segment undergoing shear was numerically simulated by particle mechanics models. Generally, the gouge particles behave in two different ways, depending on the normal stresses and rock strengths. If the normal stress is low, gouge particles can roll with the moving fracture walls, with only gentle damage at the interfaces between gouge particles and fracture surfaces. A small magnitude of shear dilation can be induced under this condition because of the roughness of fracture and gouge surfaces. When the normal stress is high, gouge particles can be crushed into a few major pieces (of large sizes) and a large number of minor comminuted particles (of small sizes). A gouge file could be formed by the comminuted gouge pieces after large shear displacement. In addition, severe damage including microcrack development and abrasion can occur on fracture walls together with the fracture closure. Therefore, not only gouge material in the fracture can influence the mechanical behavior of fractures, but also their evolution can be expected to significantly change the fluid transmissivity, flow pattern and solute transport as a result, which will be studied in future research.

The effects of microparameters on the particle mechanics models on simulated gouge behaviors were also investigated through sensitivity analysis. These parameters include the average ball radius, contact friction coefficient, mean strength and contact modulus. It was shown that the microparameters can play a key role in gouge evolution, but their behaviors can still be categorized into the two types as summarized before.

Acknowledgments Financial support from the Bolin Center for Climate Research at Stockholm University is acknowledged. Hildred Crill is thanked for helpful comments on the writing of this manuscript. Prof. Alasdair Skelton from Stockholm University and Dr. Lanru Jing from the Royal Institute of Technology (KTH) Sweden are thanked for constructive comments and discussion. Two anonymous reviewers are also greatly acknowledged for their constructive comments.

References

- Asadi MS, Rasouli V (2010) Direct shear test simulation of real rough rock fractures. In: *Proceeding of EUROCK 2010, Lausanne*, pp 231–234
- Asadi MS, Rasouli V, Barla G (2012) A bonded particle model simulation of shear strength and asperity degradation for rough rock fractures. *Rock Mech Rock Eng* 45:649–675
- Boulon M, Armand G, Hoteit N, Divoux P (2002) Experimental investigations and modeling of shear of calcite healed discontinuities of granodiorite under typical stresses. *Eng Geol* 64:117–133
- Cheng YP, Nakata Y, Bolton MD (2003) Discrete element simulation of crushable soil. *Géotechnique* 53:633–641
- Cundall PA (1999) Numerical experiments on rough joints in shear using a bonded particle model. In: Lener FK, Urai JI (eds) *Aspects of tectonic faulting*. Springer, Berlin, pp 1–9
- Duriez J, Darve F, Donzé FV (2010) A discrete modeling-based constitutive relation for infilled rock joints. *Int J Rock Mech Min Sci* 48:458–468
- Haggert L, Cox SJD, Jessell MW (1992) Observation of fault gouge development in laboratory seen through experiments. *Tectonophysics* 204:123–136
- Itasca Consulting Group Inc (2008) *PFC2D user's guide*, Minneapolis, MN
- Jaeger JC, Cook NGW, Zimmerman RW (2007) *Fundamentals of rock mechanics*, 4th edn. Blackwell, Oxford
- Jing L, Stephansson O (2007) *Fundamentals of discrete element methods for rock engineering—theory and application*. Elsevier, Amsterdam
- Lobo-Guerrero S, Vallejo LE (2005) Crushing a weak granular material: experimental numerical analyses. *Géotechnique* 55:245–249
- Mair K, Abe S (2008) 3D numerical simulations of fault gouge evolution during shear: grain size reduction and strain location. *Earth Planet Sci Lett* 274:72–81
- McDowell GR, Harireche O (2002) Discrete element modelling of soil particle fracture. *Géotechnique* 52:131–135
- Papaliangas T, Hencher SR, Lumsden AC, Manolopoulou S (1993) The effect of frictional fill thickness on the shear strength of rock discontinuities. *Int J Rock Mech Min Sci Geomech Abstr* 30:81–91
- Park JW, Song JJ (2009) Numerical simulation of a direct shear test on a rock joint using a bonded-particle model. *Int J Rock Mech Min Sci* 46:1315–1328
- Park JW, Song JJ (2013) Numerical method for the determination of contact areas of a rock joint under normal and shear loads. *Int J Rock Mech Min Sci* 58:8–22
- Pereira JP (1997) Rolling friction and shear behavior of rock discontinuities filled with sand. *Int J Rock Mech Min Sci* 34:8–22
- Pereira JP, de Freitas MH (1993) Mechanisms of shear failure in artificial fractures of sandstone and their implication for models hydromechanical coupling. *Rock Mech Rock Eng* 26:195–214
- Potyondy DO, Cundall PA (2004) A bonded-particle model for rock. *Int J Rock Mech Min Sci* 41:1329–1364

- Sammis C, King G, Biegel R (1987) The kinematics of gouge deformation. *Pure Appl Geophys* 125:777–812
- Scholz CH (1987) Wear and gouge formation in brittle faulting. *Geology* 15:493–495
- Togo T, Simamoto T (2012) Energy partition for grain crushing in quartz gouge during subseismic to seismic fault motion: an experimental study. *J Struct Geol* 38:139–155
- Wang J, Yan H (2011) One the role of particle breakage in the shear failure behavior of granular soils by DEM. *Int J Numer Anal Methods Geomech.* doi:[10.1002/nag.1124](https://doi.org/10.1002/nag.1124)
- Wang C, Tannant DD, Lilly PA (2003) Numerical analysis of the stability of heavily jointed rock slopes using PFC2D. *Int J Rock Mech Min Sci* 40:415–424
- Zhao Z, Jing L, Neretnieks I (2012) Particle mechanics model for the effects of shear on solute retardation coefficient in rock fractures. *Int J Rock Mech Min Sci* 52:92–102